Potential Energy Surface for Ground-State H_2S via Scaling of the External Correlation, Comparison with Extrapolation to Complete Basis Set Limit, and Use in Reaction Dynamics

Y. Z. Song, P. J. S. B. Caridade, and A. J. C. Varandas*

Departamento de Química, Universidade de Coimbra 3004-535 Coimbra, Portugal

Received: April 24, 2009; Revised Manuscript Received: June 26, 2009

A global double many-body expansion potential energy surface is reported for the electronic ground state of H_2S by fitting accurate ab initio energies calculated at the multireference configuration interaction level with the aug-cc-pV*QZ* basis set, after slightly correcting semiempirically the dynamical correlation by the double many-body expansion-scaled external correlation method. The function so obtained has been compared in detail with a potential energy surface of the same type recently reported (Song, Y. Z.; Varandas, A. J. C. *J. Chem. Phys.* **2009**, *130*, 134317.) by extrapolating the calculated raw energies to the complete basis set limit, eschewing any use of information alien to ab initio theory. The new potential energy surface is also used for studying the dynamics and kinetics of the $S(^1D) + H_2/D_2/HD$ reactions.

1. Introduction

The $S(^1D,^3P) + H_2$ reaction and its isotopic variants have been the subject of considerable theoretical and experimental work due to its major role in environmental issues, particularly in areas such as acid rain, air pollution, and global climate change. Specifically, the reactions of $S(^1D)$ with H_2 and its isotopomers are known to proceed via an insertion pathway, as demonstrated in many experimental observations[1−4] and theoretical work.[5−12] In a series of experiments, Inagaki et al.[1] measured Doppler profiles of H and D atoms from the reaction $S(^1D) + HD$ by a laser-induced fluorescence technique with a vacuum ultraviolet laser. They have observed an isotopic channel branching ratio of $\phi(SD + H)/\phi(SH + D) = 0.9 \pm 0.1$ for the reaction of $S(^1D) + HD$ at an average collision energy of 1.2 kcal mol^{-1}. Such a measured branching ratio and translational energy release suggest that the reaction proceeds by insertion via formation of a long-lived complex. In turn, Lee et al.[2−4] measured the integral cross sections (ICSs) and vibrational state-resolved differential cross-sections (DCSs) for the $S(^1D) + H_2/D_2/HD$ reactions at several collision energies and found that the ICSs decay monotonically with collision energy.

Theoretically, much research has been done on the potential energy surface (PES) and dynamics for the reaction $S(^1D) + H_2$.[5−13] Specifically, Zyubin et al.[6] obtained the electronic ground-state PES by fitting a grid of over 2000 points using the reproducing kernel Hilbert space (RKHS) approach and a many-body expansion[14] of the energy. The results indicate a barrierless insertion pathway along the T-shaped geometry and a 8 kcal mol^{-1} barrier for abstraction along a collinear path. Subsequently, Chao et al.[7] reported an extensive quasiclassical trajectory (QCT) study of the $S(^1D) + H_2/D_2/HD$ reactions using the PES of Zyubin et al.,[6] which qualitatively reproduced the nearly symmetric forward/backward DCSs, the monotonically decaying ICSs, and the product internal state distributions observed in the experiments.[2−4] Later, Ho et al.[8] provided a new interpolation of the ab initio data of Zyubin et al.[6] to obtain an improved PES by fitting the same set of ab initio data, which also indicates a barrierless insertion path along the T-shape geometry. Recently, Lin et al.[12] carried out quantum statistical and wave packet dynamics studies of the title reaction. The total ICSs have been predicted to decay monotonically with collision energy, thus supporting a barrierless insertion mechanism. Most recently,[15] we reported a PES for ground-state H_2S by fitting accurate ab initio energies calculated using Dunning's[16,17] aug-cc-pV*TZ* and aug-cc-pV*QZ* (simply, AV*TZ*, and AV*QZ*) basis sets via extrapolation of the electron correlation energy to the complete basis set limit (CBS) plus extrapolation to CBS of the complete-active-space self-consistent field energy (this PES will be denoted hereafter as DMBE/CBS). Exploratory dynamics calculations on the DMBE/CBS PES led to a prediction of 0.71 for the intramolecular isotope effect ($\Gamma_{intra} = k_{SH+D}/k_{SD+H}$) for $S(^1D) + HD$, which reproduces the recent experimental result of $\Gamma_{intra} = 0.72 \pm 0.07$ by Lee and Liu.[2]

In this work, we report a realistic global PES for $H_2S(^1A')$ based on DMBE[18−22] theory that is calibrated from 1972 ab initio points calculated at the multireference configuration interaction (MRCI)[23] level using the full valence complete active space (FVCAS)[24] reference function with the AV*QZ* basis set. The calculated ab initio energies are then corrected semiempirically using the double many-body expansion-scaled external correlation method (DMBE-SEC)[25] method to extrapolate to the limit of a one-electron CBS and full CI expansion and are subsequently modeled using DMBE theory. As usual, the resulting PES (DMBE/SEC) shows the correct long-range behavior at all dissociation channels, while providing an accurate fit of the calculated data at all separations.

The paper is organized as follows. Section 2 reports the ab initio calculations, and section 3 reports the formalism used for the analytical modeling. The discussion of its major topographical features is in section 4, while section 5 probes its dynamics performance when used to calculate thermal rate constants and vibrational state-resolved ICSs. The concluding remarks are in section 6.

2. Ab Initio Calculations and Scaling of the External Correlation

The ab initio calculations have been carried out at the MRCI[23] level using the FVCAS[24] wave function as a reference and Dunning's[16,17] AV*QZ* basis set. All calculations have been

* To whom correspondence should be addressed. E-mail: varandas@qtvs1.qui.uc.pt.

10.1021/jp903790h CCC: $40.75
Published on Web 07/22/2009

performed with the Molpro[26] package for electronic structure calculations. A grid of 1972 raw ab initio points has been chosen to map the PES over the S−H_2 region defined by $1.4 \le R_{H_2}/a_0 \le 3.4$, $1 \le r_{S-H_2}/a_0 \le 10$, and $0 \le \gamma/\text{deg} \le 90$. For the H−SH regions, a grid defined by $2.0 \le R_{SH}/a_0 \le 3.6$, $1 \le r_{H-SH}/a_0 \le 10$, and $0 \le \gamma/\text{deg} \le 180$ has been chosen. As usual, r, R, and γ are atom−diatom Jacobi coordinates for the relevant channel.

The raw ab initio energies calculated above have been subsequently corrected semiempirically with the DMBE-SEC[25] method such as to account for electronic excitations beyond singles and doubles and, most importantly, for the incompleteness of the basis set. The total DMBE-SEC interaction energy assumes the form

$$V(\mathbf{R}) = V_{\text{FVCAS}}(\mathbf{R}) + V_{\text{SEC}}(\mathbf{R}) \tag{1}$$

where

$$V_{\text{FVCAS}}(\mathbf{R}) = \sum_{\text{AB}} V^{(2)}_{\text{AB,FVCAS}}(R_{\text{AB}}) + V^{(3)}_{\text{ABC,FVCAS}}(R_{\text{AB}}, R_{\text{BC}}, R_{\text{AC}}) \tag{2}$$

$$V_{\text{SEC}}(\mathbf{R}) = \sum_{\text{AB}} V^{(2)}_{\text{AB,SEC}}(R_{\text{AB}}) + V^{(3)}_{\text{ABC,SEC}}(R_{\text{AB}}, R_{\text{BC}}, R_{\text{AC}}) \tag{3}$$

with $\mathbf{R} = \{R_{\text{AB}}, R_{\text{BC}}, R_{\text{AC}}\}$ being a collective variable of all internuclear distances. Explicitly, the terms in eq 3 assume the form:

$$V^{(2)}_{\text{AB,SEC}}(R_{\text{AB}}) = \frac{V^{(2)}_{\text{AB,FVCAS−CISD}}(R_{\text{AB}}) - V^{(2)}_{\text{AB,FVCAS}}(R_{\text{AB}})}{F^{(2)}_{\text{AB}}} \tag{4}$$

$$V^{(3)}_{\text{ABC,SEC}}(\mathbf{R}) = \frac{V^{(2)}_{\text{AB,FVCAS−CISD}}(\mathbf{R}) - V^{(3)}_{\text{ABC,FVCAS}}(\mathbf{R})}{F^{(3)}_{\text{ABC}}} \tag{5}$$

Following previous work,[25] $F^{(2)}_{\text{AB}}$ in eq 4 has been chosen to reproduce the bond dissociation energy of the corresponding AB diatomic, while $F^{(3)}_{\text{ABC}}$ in eq 5 has been estimated as the average of the three two-body F factors. For the AVQZ basis set, such a procedure yields $F^{(2)}_{\text{HH}} = 0.9773$, $F^{(2)}_{\text{SH}} = 0.8877$, and $F^{(3)}_{\text{SHH}} = 0.9176$.

3. Double Many-Body Expansion Representation

Within the framework of DMBE theory,[18−22] a single-sheeted PES for $SH_2(^1A')$ assumes the form

$$V(\mathbf{R}) = V^{(1)}_{S(^1D)} f(\mathbf{R}) + \sum_{i=1}^{3} \left[V^{(2)}_{\text{EHF}}(R_i) + V^{(2)}_{\text{dc}}(R_i)\right] + V^{(3)}_{\text{EHF}}(\mathbf{R}) + V^{(3)}_{\text{dc}}(\mathbf{R}) \tag{6}$$

where $V^{(1)}_{S(^1D)}$ is the energy difference between the ^1D and ^3P states of atomic sulfur: $V^{(1)}_{S(^1D)} = 0.0431045 E_{\text{h}}$, and $f(\mathbf{R})$ is a switching function that warrants the correct behavior at the $H_2(X^1\Sigma_g^+)$ + S(^1D) and SH($X^2\Pi$) + H(^2S) dissociation limits. In turn, the two- and three-body energy terms are split into extended Hartree−Fock (EHF) and dynamical correlation (dc) contributions. Because the formalism is close to the one used for the DMBE/CBS[15] PES, only a brief sketch will be presented here (see also refs 27 and 28).

3.1. Dissociation Scheme and One-Body Switching Function. The title system has the following dissociation scheme:

$$H_2S(^1A') \rightarrow H_2(X^1\Sigma_g^+) + S(^1D) \tag{7}$$

$$\rightarrow SH(X^2\Pi) + H(^2S) \tag{8}$$

Because SH($X^2\Pi$) dissociates to ground-state atoms, S(^3P) and H(^2S), it is necessary to introduce a function to remove S(^1D) from this channel. Following ref 27, this is accomplished by using the switching function

$$f(\mathbf{R}) = g(r_1)h(R_1) \tag{9}$$

with the parameters in $g(r_1)$ being chosen such as to warrant that its main effect occurs for S−H_2 distances larger than $8a_0$ or so (see the right-hand side panel of Figure 1 in the Supporting Information). In turn, the parameters in $h(R_1)$ are calibrated from a least-squares fit to an extra set of 10 AVQZ points that control the S(^1D) − S(^3P) decay with a growing H−H distance (see the left-hand side panel of Figure 1 in the Supporting Information). All parameters in eq 9 are numerically defined in Table 1 of the Supporting Information.

3.2. Two-Body Energy Terms. The potential energy curves of the diatomic fragments have been modeled with the EHF approximate correlation energy method including the united atom limit (EHFACE2U),[29] which shows the correct behavior at the asymptotes $R \rightarrow 0$ and $R \rightarrow \infty$. Specifically, the EHF part assumes the form:

$$V_{\text{EHF}}(R) = -\frac{D}{R}\left(1 + \sum_{i=1}^{n} a_i r^i\right)\exp(-\gamma r) \tag{10}$$

where $\gamma = \gamma_0[1 + \gamma_1 \tanh(\gamma_2 r)]$, and $r = R - R_e$ the displacement from the equilibrium diatomic geometry. In turn, the dc part is written as[30]

$$V_{\text{dc}}(R) = -\sum_{n=6,8,10} C_n \chi_n(R) R^{-n} \tag{11}$$

where C_n are dispersion coefficients and χ_n are damping functions. For $H_2(X\ ^1\Sigma_g^+)$, we will utilize the accurate potential energy curve of ref 28, while SH($X\ ^2\Pi$) is modeled from our own ab initio energies and the experimental dissociation energy.[31,32] The relevant numerical data are gathered in Table 2 of the Supporting Information. Because the $H_2(X\ ^1\Sigma_g^+)$ potential function is examined in detail elsewhere,[28] Figure 2 of Supporting Information illustrates only SH($X\ ^2\Pi$), which is seen to mimic accurately the calculated ab initio energies.

3.3. Three-Body Energy Terms. ***3.3.1. Three-Body dc Energy.*** The three-body dc energy assumes the usual form of a summation in inverse powers of the fragment separation distances[28]

$$V_{dc}^{(3)} = -\sum_i \sum_n f_i(\mathbf{R})\chi_n(r_i)C_n^{(i)}(R_i, \theta_i)r_i^{-n} \qquad (12)$$

where the first summation runs over all atom−diatom interactions (e.g., $i \equiv A - BC$), and $f_i(\mathbf{R}) = 1/2\{1 - \tanh[\xi(\eta R_i - R_j - R_k)]\}$ and $\chi_n(r_i)$ are damping functions.[28] In turn, R_i is the internuclear distance for the i-th pair, r_i is the corresponding atom−diatom (center-of-mass), and θ_i is the angle between $\vec{r}_i$ and $\vec{R}_i$ (see Figure 1 of ref 33). Following recent work,[27] we have fixed $\eta = 6$ and $\xi = 1.0a_0^{-1}$. All of the numerical values of the parameters in eq 12 are collected in Table 3 of the Supporting Information, while their internuclear dependences are displayed in Figure 3 of the Supporting Information.

3.3.2. Three-Body EHF Energy. For a given triatomic geometry, the total three-body energy is obtained by subtracting the sum of the one- and two-body energies from the corresponding DMBE-SEC energies in eq 6. Then, by removing the three-body dc part described in eq 12 from the total three-body energy, the three-body EHF energy is obtained. This is finally modeled by using the following three-body distributed-polynomial[34] form

$$V_{EHF}^{(3)} = \sum_{j=1}^{2} P_j(Q_1, Q_2, Q_3) \times \prod_{i=1}^{3} \{1 - \tanh[\gamma_i^j(R_i - R_i^{j,ref})]\} \qquad (13)$$

where $P_j(Q_1, Q_2, Q_3)$ ($j = 1, 2$) is a polynomial up to six-order in the popular D_{3h} symmetry coordinates.[14,35,36] As usual, we obtain the reference geometries $R_i^{j,ref}$ by first assuming their values to coincide with bond distances of the associated stationary points. Subsequently, this condition is relaxed by a trial-and-error least-squares fitting procedure. Similarly, the nonlinear range-determining parameters γ_i^j have been optimized in this way. The complete set of parameters amounts to a total of 100 linear coefficients c_i, six nonlinear coefficients γ_i^j, and six reference geometries $R_i^{j,ref}$. All numerical values of the least-squares parameters are gathered in Tables 4 and 5 of the Supporting Information. Table 1 shows the stratified root-mean-squared deviations (rmsd) of the final PES with respect to all of the fitted ab initio energies. A total of 1972 points covering a range of energy up to ~2500 kcal mol^{-1} above the H_2S global minimum have been utilized for the calibration procedure, with a total rmsd of 0.86 kcal mol^{-1}.

TABLE 1: Stratified Root-Mean-Square Deviations of the DMBE/SEC PES

energy[a]	N[b]	rmsd[a]	$N_{>rmsd}$[c]
10	41	0.096	7
20	55	0.125	13
30	85	0.385	10
40	115	0.458	16
50	145	0.567	23
60	185	0.572	32
80	306	0.636	67
100	767	0.601	146
150	1474	0.741	319
200	1769	0.768	386
250	1799	0.778	395
500	1877	0.817	410
1000	1942	0.840	435
1500	1959	0.855	440
2000	1963	0.855	442
2500	1972	0.862	444

[a] The units of energy and rmsd are kcal mol^{-1}. [b] Number of points in the indicated energy range. [c] Number of points with an energy deviation larger than the rmsd.

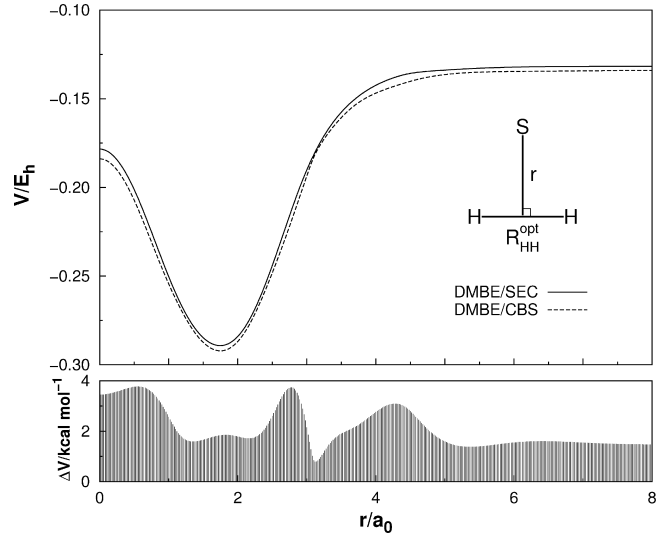

Figure 1. Approximate minimum energy path as a function of r (distance between the S atom and the center of the HH diatom), with the HH bond length optimized at each value of r.

4. Features of the DMBE/SEC PES

The approximate minimum energy path of the DMBE/SEC PES is displayed in Figure 1 as a function of r, which measures the distance between the S atom and the center of the HH diatomic, with the bond length of HH being optimized at each value of r. Also shown for comparison in this figure is the corresponding path of the accurate DMBE/CBS PES recently reported.[15] The first visible feature is the absence of a barrier for the perpendicular insertion of the S(^2D) atom into the HH diatom. Also apparent is the parallelism between the minimum energy paths of the DMBE/SEC and DMBE/CBS PESs. This is quite pleasing, since they correspond to optimized paths and the pragmatic DMBE-SEC method only corrects the dc at the equilibrium geometry of the relevant fragments. A similar remark can be made from Figure 2, which shows the optimized C_{2v} bending curve of H_2S as a function of bending angle, with the bond distance of SH optimized at each angle. Note that the barrier to linearity calculated from the DMBE/SEC PES is 24296 cm^{-1}, thus, only 28 cm^{-1} larger than the value of 24268 cm^{-1} calculated by Tarczay et al.[37] It may also be compared with the value of 23753 cm^{-1} for DMBE/CBS, which is predicted to be only 543 cm^{-1} higher.

The near parallel behavior of the DMBE/SEC and DMBE/CBS PESs is highlighted in the bottom panels of Figures 1 and 2, with the DMBE/CBS predicting a slightly deeper well depth than the DMBE/SEC PES. As noted above, this may largely be due to the fact that the DMBE-SEC method employs a single constant scaling factor (approximated by the average of the three diatom scaling factors) for all of the points calculated with the AVQZ basis set. It may also be due to the fact that the MRCI energies utilized to calibrate the DMBE/SEC form have not included the Davidson correction. This suggests that the DMBE-SEC scheme slightly underestimates such a popular correction, a finding also supported from our recent work on the NH_2 system.[27] Quantitatively, the energy difference at the global minimum in Figures 1 and 2 amounts to ~2 kcal mol^{-1}, with the well depths calculated relative to the three-atom dissociation limit being $-0.2892E_h$ and $-0.2921E_h$, respectively, for the DMBE/SEC and DMBE/CBS PESs. Thus, the well depth at

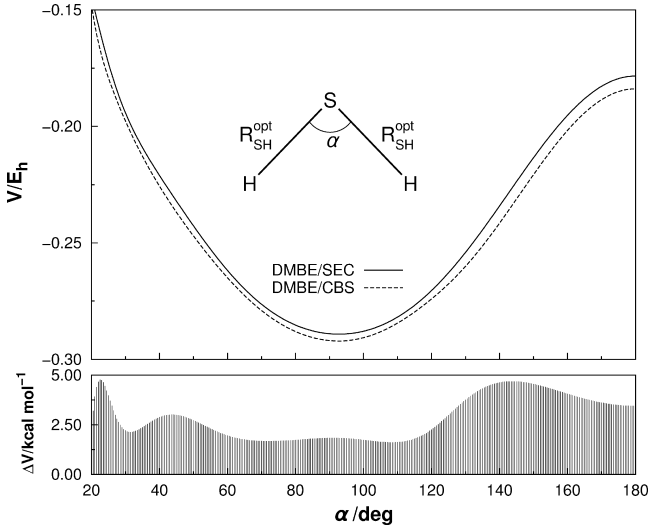

Figure 2. Optimized C_{2v} bending curve of H_2S as a function of bending angle, with the bond distance of SH optimized at each bending angle.

TABLE 2: Stationary Points of the H_2S PES[a]

feature	R_1/a_0	R_2/a_0	R_3/a_0	E/E_h[b]	ΔV[c]	ω_1	ω_2	ω_3
global minimum								
DMBE/SEC[d]	3.6623	2.5295	2.5295	−0.2892	−99.04	2643	2684	1147
exp.[e]	3.6142	2.5096	2.5096		−99.10	2615	2626	1183
ab initio[f]	3.6728	2.5409	2.5409		−98.70	2683	2696	1183
RKHS[g]	3.6481	2.5293	2.5293	−0.2867	−98.57	2709	2777	1200
DMBE/CBS[h]	3.6615	2.5320	2.5320	−0.2921	−99.30	2665	2691	1199
stationary points[d]								
H−S−H	4.9094	2.4547	2.4547	−0.1785	−29.57	3151	3186	1510*i*
H−S···H	6.3389	2.5624	3.7765	−0.1164	9.39	2477	1444*i*	1123*i*
S−H···H	2.0665	2.6758	4.7423	−0.1217	6.07	1462	1618*i*	919*i*

[a] Harmonic frequencies in cm^{-1}. [b] Energy relative to the three-atom limit S + H + H. [c] Relative to the $S(^1D) + H_2$ asymptote (in kcal mol^{-1}). [d] This work. [e] Experimental values.[42] [f] Ab initio calculation from ref 6. [g] Calculated using RKHS PES.[8] [h] Calculated using DMBE/CBS PES.[15]

equilibrium H_2S is enhanced by $\sim 0.0038E_h$ ($\sim$2.38 kcal mol^{-1}) by the Davidson correction. In fact, if this is not included for the AV*TZ* and AV*QZ* energies, the well depth extrapolated to CBS limit is $0.2921 - 0.0038 = 0.2883E_h$, thus only $\sim$0.56 kcal mol^{-1} smaller than the well depth of the DMBE/SEC PES. This result also corroborates the high reliability and consistency of the CBS and DMBE-SEC methods.

The characterization of the global minimum and other stationary points (geometry, energy, and vibrational frequencies) is shown in Table 2. The global minimum is located at $R_1 = 3.6623a_0$ and $R_2 = R_3 = 2.5295a_0$, which shows a maximum deviation of only $0.0025a_0$ for the SH bond length (R_2 and R_3) when compared with the results for the DMBE/CBS PES ($R_1 = 3.6615a_0$, and $R_2 = R_3 = 2.5320a_0$).

Figures 3−7 illustrate the major topographical features of the H_2S DMBE/SEC PES reported in the present work. The salient features are the most relevant stationary points of the title system. They also illustrate its smooth and correct behavior over the whole configuration space, including the long-range regions, clearly an asset of DMBE theory. Besides the global minimum at $r_{S-H_2} \approx 1.8a_0$ and $r_{HH} \approx 3.6a_0$, Figure 3 also shows that the sulfur atom approaches H_2 from large atom−diatom separations along T-shaped geometries via a barrierless process, thus agreeing with previous findings for the DMBE/CBS[15] PES and the recent theoretical work of Zyubin et al.[6] and Ho et al.[8]

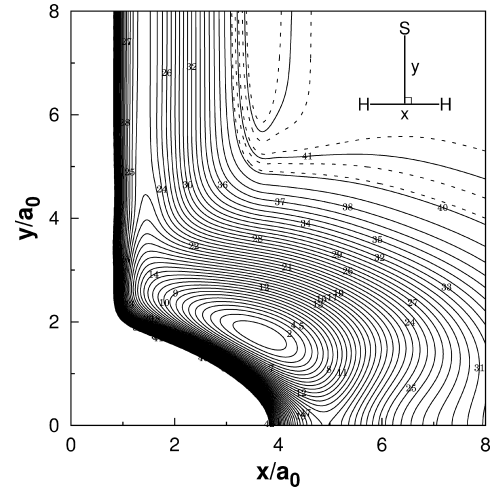

Figure 3. Contour plot for the C_{2v} insertion of the S atom into H_2. Contours are equally spaced by $0.0075E_h$, starting at $-0.280E_h$. The dashed areas are contours equally spaced by $0.004E_h$, starting at $-0.0095E_h$.

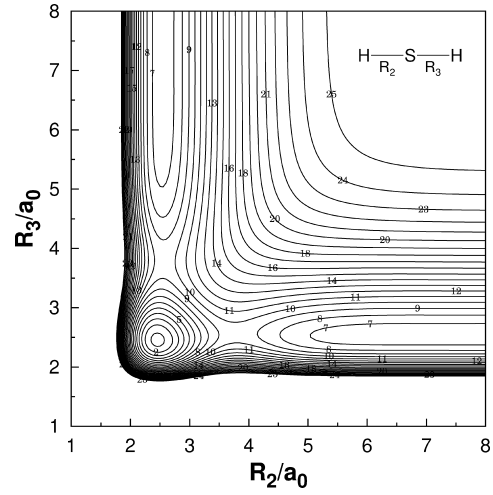

Figure 4. Contour plot for bond stretching in linear H−S−H. Contours are equally spaced by $0.007E_h$, starting at $-0.175E_h$.

Figure 4 shows a contour plot for linear H−S−H stretch. The notable feature from this plot is the existence of a H−S−H linear saddle point located at $r_{SH} = 2.4547a_0$ with an energy of 69.47 kcal mol^{-1} above the global minimum of H_2S but still 29.57 kcal mol^{-1} below the energy of the $S(^1D) + H_2$ asymptote. This compares well with the DMBE/CBS PES, where the saddle point is predicted to occur at $r_{SH} = 2.4860a_0$ with an energy of 67.90 kcal mol^{-1} above the global minimum and 31.40 kcal mol^{-1} below the reactants asymptote. Also visible from this plot is an H−S···H saddle point located at $R_2 = 2.5624a_0$ and $R_3 = 3.7765a_0$ with an energy of 9.39 kcal mol^{-1} higher than the energy of $S(^1D) + H_2$; see Table 2. The major features of the DMBE/SEC PES for collinear S−H−H are illustrated in Figure 5. As seen, the collinear saddle point is found to have a geometry with $r_{SH} = 2.6758a_0$ and $r_{HH} = 2.0665a_0$ and a barrier height of 6.07 kcal mol^{-1}. This compares with the homologous values of $r_{SH} = 2.7223a_0$, $r_{HH} = 2.0723a_0$, and 5.81 kcal mol^{-1} for the DMBE/CBS PES. Although the DMBE/CBS PES predicts a slightly deeper global minimum and smaller barrier heights for the saddle points than the DMBE/SEC PES, their location is very similar with a maximum deviation of $0.063a_0$ for the HH bond length of the H−S−H linear saddle point.

Figure 6 shows energy contours for the S atom moving around ground-state H_2 whose bond length is fixed at its equilibrium

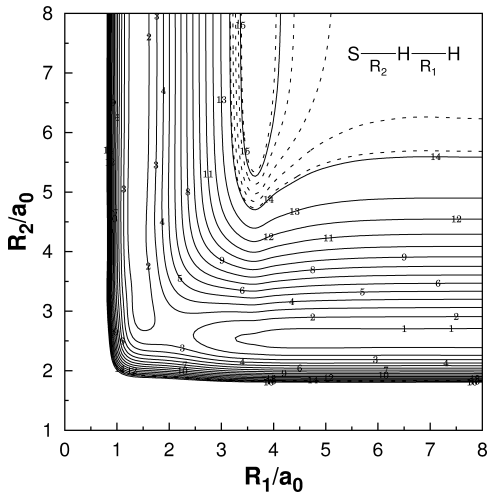

Figure 5. Contour plot for bond stretching in linear S−H−H. Contours are equally spaced by $0.01E_h$, starting at $-0.135E_h$. The dashed area shows contours equally spaced by $0.0025E_h$, starting at $-0.00425E_h$.

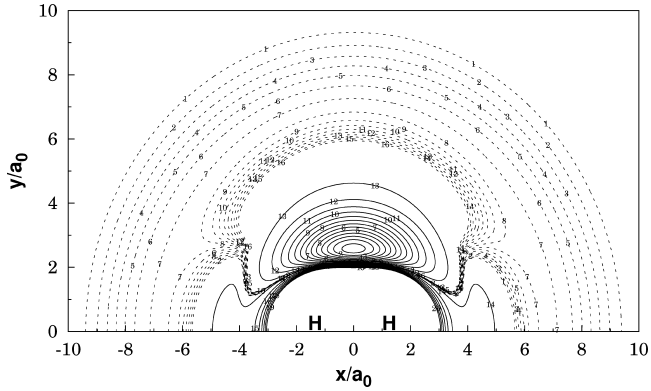

Figure 6. Contour plot for the S atom moving around a fixed H_2 diatom in equilibrium geometry $R_{H_2} = 1.401a_0$, which lies along the *X*-axis with the center of the bond fixed at the origin. Contours are equally spaced by $0.0045E_h$, starting at $-0.189E_h$. The dashed areas are contours equally spaced by $-0.00008E_h$, starting at $-0.13155E_h$.

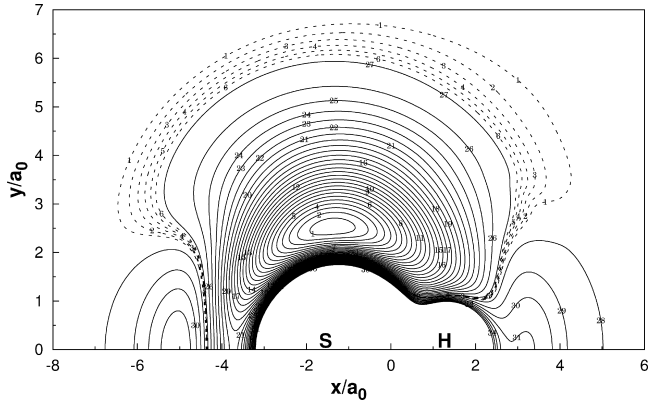

Figure 7. Contour plot for the H atom moving around SH whose bond length is fixed at $R_{SH} = 2.534a_0$ and lies along the *X*-axis with the center of the bond fixed at the origin. Contours are equally spaced by $0.0055E_h$, starting at $-0.2855E_h$. The dashed lines show contours equally spaced by $-0.00045E_h$, starting at $-0.13935E_h$.

geometry of $r_{HH} = 1.401a_0$. The corresponding plot for the H atom moving around the SH diatom with its bond distance fixed at $r_{SH} = 2.534a_0$ is shown in Figure 7. The two plots clearly reveal a smooth behavior at both short and long-range regions. Another important aspect of Figure 7 is the existence of a Σ/Π conical intersection for collinear S−H−H geometries, since H_2S may dissociate to SH($X\ ^2\Pi$) + H(^2S) and SH($A\ ^2\Sigma^+$) + H(^2S). Similarly to DMBE/CBS, the DMBE/SEC PES cannot describe the crossing due to being single-sheeted. The full implications of this on dynamics of the title reaction cannot be anticipated, although available results suggest that they are probably minor.

TABLE 3: Least-Squares Parameters in Eq 14 for S + H_2/D_2/HD Reaction Rate Constants

reaction	A (cm^3 s^{-1} K^{-n})	n	B (K)
S + H_2 → SH + H	3.08×10^{-11}	0.25	13.20
S + D_2 → SD + D	3.71×10^{-11}	0.18	12.44
S + HD → SH + D	1.19×10^{-11}	0.27	13.12
S + HD → SD + H	2.06×10^{-11}	0.17	12.48

5. Dynamics of S(^1D) + H_2/D_2/HD Reactions

5.1. Thermal Rate Coefficients. This section presents the results of dynamics calculations using the DMBE/SEC function described in the present work. First, we report QCT calculations of the thermal rate coefficients (or constants) for the S(^1D) + H_2/D_2/HD reactions over the temperature range $300 \le T/K \le 3000$ by running a total of 5000 trajectories per temperature with an adapted version of the VENUS96[38] code. For this, the rovibrational state of the H_2 molecule has been sampled according to the procedure of ref 39 but with the rovibrational partition function weighted for the ortho−para symmetry of the hydrogen molecule. An integration step size of 1.5×10^{-16} s has been chosen such as to warrant conservation of the total

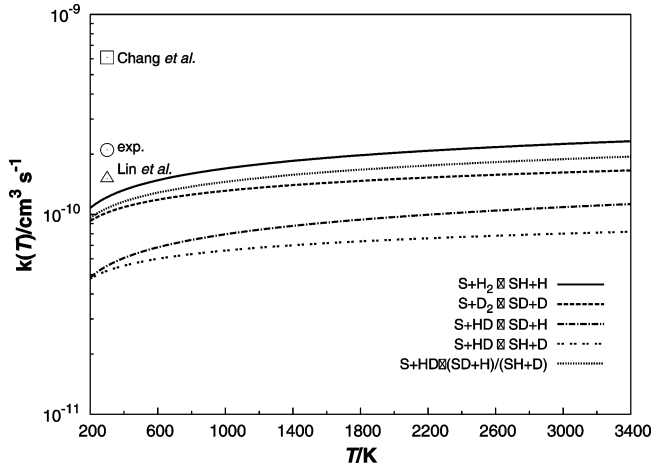

Figure 8. Temperature dependence of thermal rate constants for the S(^1D) + H_2/D_2/HD reactions. Note that the dotted line shows the thermal rate constants for S(^1D) + HD reactions with the products being either SD + H or SH + D.

TABLE 4: ICS σ (in Å^2) for the S(^1D) + H_2($v = 0, j = 0$) Reaction at 2.24 and 3.96 kcal mol^{-1} Collision Energy[a]

	total		$v' = 0$		$v' = 1$		v' branching ratio	
method (PES)	$j = 0$	$j = 1$	$j = 0$	$j = 1$	$j = 0$	$j = 1$	$j = 0$	$j = 1$
			$E_c = 2.24$ kcal mol^{-1}					
MGB(DMBE/SEC)	26.09	26.15	20.69	20.14	5.40	6.01	0.26	0.30
QM(RKHS)[b]	27.21	27.42	24.17	23.63	3.04	3.79	0.13	0.16
HB(RKHS)[b]	24.28	25.70	20.40	21.09	3.88	4.61	0.19	0.22
GB(RKHS)[b]	22.85	24.45	20.88	21.55	1.97	2.90	0.09	0.13
			$E_c = 3.96$ kcal mol^{-1}					
MGB(DMBE/SEC)	24.16	23.76	18.02	17.55	6.14	6.21	0.34	0.35
HB(RKHS)[b]	22.06	22.14	17.45	17.30	4.61	4.84	0.26	0.22
GB(RKHS)[b]	21.76	21.99	18.01	17.88	3.74	4.11	0.21	0.23

[a] The vibrational branching ratio is defined as $\sigma(v' = 1)/\sigma(v' = 0)$. [b] From ref 10.

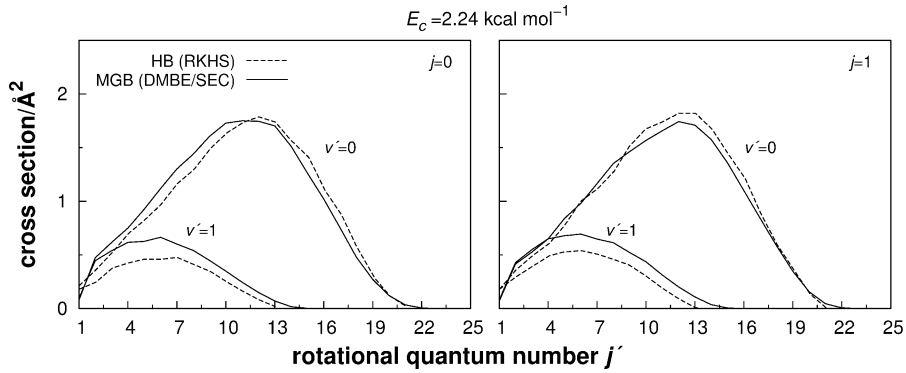

Figure 9. Vibrational state-resolved ICSs calculated for S(^1D) + H_2($v = 0$, $j = 0$, 1) reaction at $E_c = 2.24$ kcal mol^{-1}. Left panel, $j = 0$; right panel, $j = 1$.

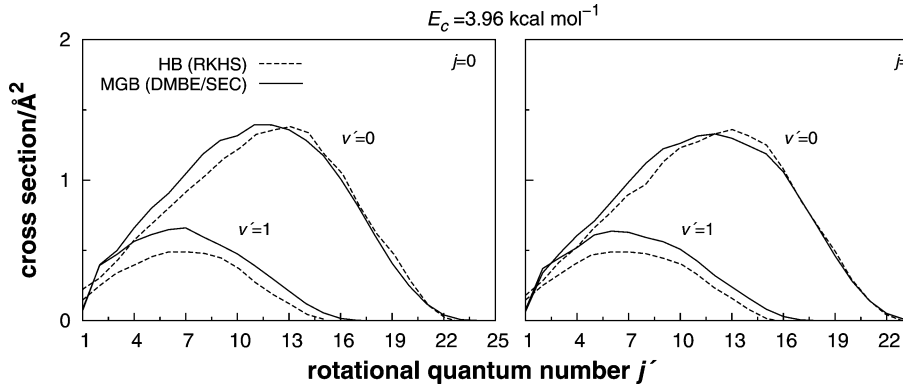

Figure 10. Vibrational state-resolved ICSs calculated for S(^1D) + H_2($v = 0$, $j = 0$, 1) reaction at $E_c = 3.96$ kcal mol^{-1}. Left panel, $j = 0$; right panel, $j = 1$.

energy to better than one part in 10^3. The trajectories are started at an atom−diatom distance of 9 Å, a value sufficiently large to make the interaction energy essentially negligible. To model the temperature dependence of the calculated rate constants, a three-parameter Arrhenius form has been utilized,

$$k(T) = AT^n \exp\left(-\frac{B}{T}\right) \tag{14}$$

with all parameters being numerically defined in Table 3. Figure 8 illustrates the temperature dependence of the calculated thermal rate coefficients for the three isotopic reactions here studied. They are found to be ordered for the various isotopes as $k_{H_2} > k_{HD} > k_{D_2}$, at all temperatures. For the S(^1D) + H_2 reaction at 300 K, the rate constant is found to be 1.22×10^{-10} cm^3 s^{-1} and, thus, is in reasonably good agreement with experiment[40] (2.1×10^{-10} cm^3 s^{-1}) and the quantum statistical results (1.51×10^{-10} cm^3 s^{-1} for *para*-H_2; 1.48×10^{-10} cm^3 s^{-1} for *ortho*-H_2) of Lin and Guo.[12] The thermal rate constants for S(^1D) + HD reaction forming SH + D and SD + H products are predicted to be 0.53×10^{-10} and 0.55×10^{-10} cm^3 s^{-1}, respectively. Thus, the intramolecular isotope effect is $\Gamma_{intra} = k_{SH+D}/k_{SD+H} = 0.96$, which is slightly larger than the value of 0.71 obtained from DMBE/CBS PES[15] and the Lee and Liu[2,3] experimental result of 0.72 ± 0.07 but is close to the experimental value of 0.9 ± 0.1 obtained by Inagaki et al.[1] and the QCT result of 0.93 of Bañares et al.[11]

5.2. ICSs. By running batches of 10^5 trajectories at collision energies of 2.24 and 3.96 kcal mol^{-1}, vibrational state-resolved ICSs have also been calculated for the S(^1D) + H_2($v = 0$, $j = 0$, 1) reaction. The calculated total and v' state-resolved ICSs are gathered in Table 4. At the collision energy 2.24 kcal mol^{-1}, the total ICSs obtained from our DMBE/SEC PES are found to be in good overall agreement with the results calculated by Bañares et al.[10] with quantum mechanical, QCT histogramatic binning, and QCT Gaussian-weighted binning methods using the RKHS PES of Ho et al.[8] denoted (together with the PES where they have been used) as QM(RKHS), HB(RKHS), and GB(RKHS), respectively. Perhaps more interesting is a comparison of the vibrational state-resolved ICSs. These have been calculated here with the momentum Gaussian-binning[41] method, MGB(DMBE/SEC).

Figure 9 shows the MGB(DMBE/SEC) product rotational distributions for the S(^1D) + H_2($v = 0$, $j = 0$, 1) reactions calculated at a collision energy of 2.24 kcal mol^{-1}. Also shown by the dashed line are the HB(RKHS) results of Bañares et al.[10] The MGB(DMBE/SEC) distribution is seen to peak at $j' = 11$ and $j' = 13$ for initial rotational states of $j = 0$ and 1, respectively, when the product is SH($v' = 0$). In turn, for the product SH($v' = 1$), the corresponding rotational distributions peak at $j' = 6$. As Figure 10 shows, the results are in good agreement with those of Bañares et al.[10] for both collisional energies.

6. Conclusions

A global single-sheeted DMBE/SEC PES has been reported for the ground state of H_2S based on a least-squares fit to a set of high level AV*QZ* ab initio energies that have been corrected by the DMBE-SEC method. The various topographical features of the new PES have been examined in detail and compared with the DMBE/CBS and other PESs, as well as experimental data available in the literature. The accuracy and consistency of the DMBE-SEC approach have also been confirmed by comparing the corrected energies with those obtained from CBS

extrapolation to the one-electron CBS limit. Finally, the QCT thermal rate constants calculated with the DMBE/SEC PES for the $S(^1D) + H_2/D_2/HD$ reactions have been shown to be in good agreement with available experimental and theoretical data and so did the vibrational state-resolved ICSs for the $S(^1D) + H_2(v = 0, j = 0, 1)$ reaction. On the basis of the above, the DMBE/SEC PES here reported may be recommended for dynamics studies of any type.

Having reported[15] another PES for the title system out of the same raw ab initio energies, one may wonder about their relative merits. As far as the accuracy of the fits is concerned, they can hardly be discriminated since they have rather similar rmsd. Of course, the DMBE/CBS PES has been constructed in a purely ab initio fashion, whereas the DMBE/SEC one here reported entails a small degree of empiricism via scaling of the external (or dynamical) correlation. The fact that they are so similar can therefore be regarded as an asset on the consistency of both schemes. Regarding the performance of the two PESs against experimental data, an answer must await until an extensive dynamics analysis that goes beyond the rate constant data is reported for both. However, even then, any superior agreement of one against the other must be qualified as discarding nonadiabatic effects due to the single-sheeted nature of both PESs. Such studies are currently in progress.

Acknowledgment. This work was supported by the Fundação para a Ciencia e Tecnoligia, Portugal.

Supporting Information Available: Tables showing parameters and numerical values and figures showing the switching function used to model the single-sheeted H_2S DMBE/SEC PES, EHFACE2U PEC for $SH(X^2\Pi)$, dispersion coefficients for the atom−diatom asymptotic channels of H_2S, and contour plot for bond stretching. This material is available free of charge via the Internet at http://pubs.acs.org.

References and Notes

(1) Inagaki, Y.; Shamsuddin, S. M.; Matsumi, Y.; Kawasaki, M. *Laser Chem.* **1994**, *14*, 235.
(2) Lee, S.-H.; Liu, K. *Chem. Phys. Lett.* **1998**, *290*, 323.
(3) Lee, S.-H.; Liu, K. *Appl. Phys. B: Laser Opt.* **2000**, *71*, 627.
(4) Lee, S.-H.; Liu, K. *J. Phys. Chem. A* **1998**, *102*, 8637.
(5) Chang, A. H. H.; Lin, S. H. *Chem. Phys. Lett.* **2000**, *320*, 161.
(6) Zyubin, A. S.; Mebel, A. M.; Mebel, M.; Chao, S. D.; Skodje, R. T. *J. Chem. Phys.* **2001**, *114*, 320.
(7) Chao, S. D.; Skodje, R. T. *J. Phys. Chem. A* **2001**, *105*, 2474.
(8) Ho, T.; Hollebeek, T.; Rabitz, H.; Chao, S. D.; Skodje, R. T.; Zyubin, A. S.; Mebel, A. M. *J. Chem. Phys.* **2002**, *116*, 4124.
(9) Maiti, B.; Schatz, G. C.; Lendvay, G. *J. Phys. Chem. A* **2004**, *108*, 8772.
(10) Bañares, L.; Aoiz, F. J.; Honvault, P.; Launay, J.-M. *J. Phys. Chem. A* **2004**, *108*, 1616.
(11) Banares, L.; Castillo, J. F.; Honvault, P.; Launay, J. *Phys. Chem. Chem. Phys.* **2005**, *7*, 627.
(12) Lin, S. Y.; Guo, H. *J. Chem. Phys.* **2005**, *122*, 074304.
(13) Song, Y. Z.; Kinal, A.; Caridade, P. J. S. B.; Varandas, A. J. C.; Piecuch, P. *J. Mol. Struct. Theochem.* **2008**, *859* (1−3), 22.
(14) Murrell, J. N.; Carter, S.; Farantos, S. C.; Huxley, P.; Varandas, A. J. C. *Molecular Potential Energy Functions*; Wiley: Chichester, 1984.
(15) Song, Y. Z.; Varandas, A. J. C. *J. Chem. Phys.* **2009**, *130*, 134317.
(16) Kendall, R. A.; Dunning, T. H., Jr.; Harrison, R. J. *J. Chem. Phys.* **1992**, *96*, 6769.
(17) Dunning, T. H., Jr. *J. Chem. Phys.* **1989**, *90*, 1007.
(18) Varandas, A. J. C. *Advanced Series in Physical Chemistry*; World Scientific Publishing: Singapore, 2004; Chapter 5, p 91.
(19) Varandas, A. J. C. *Lecture Notes in Chemistry*; Laganá, A., Riganelli, A., Eds.; Springer: Berlin, 2000; Vol. 75, p 33.
(20) Varandas, A. J. C. *Adv. Chem. Phys.* **1988**, *74*, 255.
(21) Varandas, A. J. C. *J. Mol. Struct. Theochem.* **1985**, *120*, 401.
(22) Varandas, A. J. C. *Mol. Phys.* **1984**, *53*, 1303.
(23) Werner, H. J.; Knowles, P. J. *J. Chem. Phys.* **1988**, *89*, 5803.
(24) Knowles, P. J.; Werner, H.-J. *Chem. Phys. Lett.* **1985**, *115*, 259.
(25) Varandas, A. J. C. *J. Chem. Phys.* **1989**, *90*, 4379.
(26) Werner, H. J.; Knowles, P. J.; Lindh, R.; Schütz, M.; Celani, P.; Korona, T.; Manby, F. R.; Rauhut, G.; Amos, R. D.; Bernhardsson, A.; Berning, A.; Cooper, D. L.; Deegan, M. J. O.; Dobbyn, A. J.; Eckert, F.; Hampel, C.; Hetzer, G.; Lloyd, A. W.; McNicholas, S. J.; Meyer, W.; Mura, M. E.; Nicklass, A.; Palmieri, P.; Pitzer, R.; Schumann, U.; Stoll, H.; Stone, A. J.; Tarroni, R.; Thorsteinsson, T. *Molpro 2008, a Package of Ab Initio Programs*; Cardiff, UK, 2008.
(27) Varandas, A. J. C.; Poveda, L. *Theor. Chem. Acc.* **2006**, *116*, 404.
(28) Varandas, A. J. C. *J. Chem. Phys.* **1996**, *105*, 3524.
(29) Varandas, A. J. C.; Silva, J. D. *J. Chem. Soc. Faraday Trans.* **1992**, *88*, 941.
(30) Varandas, A. J. C. *Mol. Phys.* **1987**, *60*, 527.
(31) Huber, K. P.; Herzberg, G. *Molecular Spectra and Molecular Structure Constants of Diatomic Molecules*; van Nostrand Reinhold: New York, 1979.
(32) Lodders, K. *J. Phys. Chem. Ref. Data* **2004**, *33*, 357.
(33) Varandas, A. J. C. *Chem. Phys. Lett.* **1992**, *194*, 333.
(34) Martínez-Nuñez, E.; Varandas, A. J. C. *J. Phys. Chem.* **2001**, *105*, 5923.
(35) Murrell, J. N.; Sorbie, K. S.; Varandas, A. J. C. *Mol. Phys.* **1976**, *32*, 1359.
(36) Varandas, A. J. C.; Murrell, J. N. *Faraday Discuss. Chem. Soc.* **1977**, *62*, 92.
(37) Tarczay, G.; Császár, A. G.; Leininger, M. L.; Klopper, W. *Chem. Phys. Lett.* **2000**, *322*, 119.
(38) Hase, W. L.; Duchovic, R. J.; Hu, X.; Komornicki, A.; Lim, K. F.; Lu, D.; Peslherbe, G. H.; Swamy, K. N.; Linde, S. R. V.; Varandas, A. J. C.; Wang, H.; Wolf, R. J. *QCPE Bull.* **1996**, *16*, 43.
(39) Caridade, P. J. B. S.; Varandas, A. J. C. *J. Phys. Chem. A* **2004**, *108*, 3556.
(40) Black, G.; Jusinski, L. E. *J. Chem. Phys.* **1985**, *82*, 789.
(41) Varandas, A. J. C. *Chem. Phys. Lett.* **2007**, *439*, 386.
(42) Chase, M. W., Jr.; Davies, C. A.; Downey, J. R., Jr.; Frurip, D. J.; McDonald, R. A.; Syveraud, A. N. *JANAF Thermodinamic Tables*, 3rd ed.; American Chemical Society and American Institute for Physics for the National Bureau of Standards: New York, 1985.

JP903790H